The University of Alabama in Huntsville

FINAL REPORT

Studies of Large-Area Inversion-Layer Metal-Insulator-Semiconductor (IL/MIS) Solar Cells and Arrays

(NAG8-108)

Submitted to:

George C. Marshall Space Flight Center
National Aeronautics and Space Administration
Marshall Space Flight Center, Alabama 35812

Prepared by:
Fat Duen Ho, Principal Investigator
Professor, Electrical and Computer Engineering
The University of Alabama in Huntsville
Huntsville, Alabama 35899
Phone: (205) 895-6168
Fax: (205) 895-6803

Fat Duen Ho
8/2/96

Abstract. Many inversion-layer metal-insulator-semiconductor (IL/MIS) solar cells have been fabricated. There are around eighteen 1 cm^2 IL/MIS solar cells which have efficiencies greater than 7%. There are only about three 19 cm^2 IL/MIS cells which have efficiencies greater than 4%. The more accurate control of the thickness of the thin layer of oxide between aluminum and silicon of the MIS contacts has been achieved. A lot of effort and progress have been made in this area.

A comprehensive model for MIS contacts under dark conditions has been developed that covers a wide range of parameters. It has been applied to MIS solar cells. One of the main advantages of these models is the prediction of the range of the thin oxide thickness versus the maximum efficiencies of the MIS solar cells. This is particularly important when the thickness is increased to 25Å. This study is very useful for our investigation of the IL/MIS solar cells.

The two-dimensional numerical model for the IL/MIS solar cells has been tried to develop and the results are presented in this report.

1.0 Introduction

The objectives of this study are: (1) investigation and fabrication of large area silicon inversion-layer metal-insulator-semiconductor (MIS) solar cells for use in space solar arrays; (2) continue developing a simple inexpensive process for fabricating high-efficiency IL solar cells; and (3) continue modeling the IL/MIS solar cells.

Many inversion layer MIS solar cells have been fabricated. There are around eighteen 1 cm^2 IL/MIS solar cells which have efficiencies greater than 7%. There are only about three 19 cm^2 IL/MIS cells which have efficiencies greater than 4%.

The growth of the thin layer of oxide between aluminum and silicon of the MIS contacts was one of the major tasks in this project. A lot of effort and progress have been made in this area [1,2]. The theoretical study of MIS contacts and MIS solar cells have been pursued. A comprehensive model for MIS devices has been developed. It has been applied to MIS solar cells [3,4]. This study is very useful for our investigation of the inversion-layer MIS solar cells.

The two-dimensional numerical model for the IL/MIS solar cells has been tried to develop, but it fails to yield good results.

2.0 The Fabrication of IL/MIS Solar Cells

The operational principle, the design consideration, and the fabrication of inversion-layer MIS solar cells have been presented in other papers [5,6,7,8]. The fabrication procedures of the inversion-layer MIS solar cells are briefly described as follows:

1. Silicon dioxide (SiO_2) with a thickness of approximately 1300Å is thermally grown on a <111> p-type silicon substrate.
2. The front metal contact regions are defined using the first mask. They are etched on the front surface.
3. A thin oxide layer is grown in metal contact regions.
4. Aluminum is evaporated on the back surface of the silicon substrate and followed by sintering in a 470°C furnace.
5. Aluminum is evaporated on the front side.
6. The grid patterns of the front metalization are defined by using a second mask.

We have fabricated many IL/MIS solar cells. The 1 cm^2 cells with 7% or higher efficiencies are listed in Table 1. The 1 cm^2 cells with 6% to 7% efficiencies are tabulated in Table 2. The 1 cm^2 IL/MIS solar cells with efficiencies between 4% and 6% are shown in Table 3. The large area (total area = 19.78 cm^2) IL/MIS solar cells are summarized in Table 4 [2].

Table 1. 1 CM^2 IL-MIS Solar Cells with 7% or Higher Efficiencies

Substrate Resistivity Ω-cm	Cell ID		Experimental Results			
			V_{oc} (V)	I_{sc} (mA)	FF	% EFF
1.2	8-4	A	0.567	29.050	0.444	7.003
1.2	1-1	A	0.575	30.400	0.536	8.909
		B	0.570	29.000	0.452	7.106
1.2	1-1	A	0.536	27.350	0.561	7.825
		C	0.526	27.100	0.552	7.481
0.7-1.3	13-1	A	0.562	26.200	0.546	7.646
		B	0.559	26.550	0.552	7.787
	13-2	A	0.555	26.600	0.560	7.863
		B	0.556	25.900	0.548	7.500
		C	0.548	25.300	0.561	7.402
		D	0.560	27.050	0.582	8.383
0.7-1.3	14-2	A	0.549	24.600	0.578	7.430
3.0-6.0	14-3	A	0.525	25.300	0.589	7.441
		B	0.522	24.750	0.577	7.088
		C	0.526	25.100	0.590	7.404
0.7-1.3	2-2	C	0.547	26.400	0.614	8.430
0.7-1.3	4-1	A	0.523	25.300	0.564	7.100
	4-2	C	0.536	25.850	0.612	8.067

Table 2. 1 CM^2 IL-MIS Solar Cells with 6% to 7% Efficiencies

Substrate Resistivity Ω-cm	Cell ID		Experimental Results			
			V_{oc} (V)	I_{sc} (mA)	FF	% EFF
1.2	8.3	A	0.573	29.000	0.406	6.456
		B	0.566	27.700	0.432	6.477
	8.4	C	0.557	27.450	0.453	6.628
1.2	9.3	A	0.579	30.350	0.376	6.331
		C	0.575	29.700	0.387	6.319
0.7-1.3	13-1	C	0.563	25.600	0.459	6.291
		D	0.563	25.550	0.464	6.350
0.7-1.3	14-2	B	0.546	24.750	0.544	6.994
		C	0.537	24.250	0.530	6.563
		D	0.545	24.550	0.539	6.865
3.0-6.0	14-3	D	0.524	23.800	0.577	6.849
8.0-12.0	14-5	B	0.502	26.750	0.496	6.333
		D	0.507	26.900	0.506	6.565
3.0-6.0	1-3	A	0.494	22.650	0.608	6.476
		D	0.496	22.950	0.645	6.986
0.7-1.3	2-1	A	0.523	24.800	0.546	6.737
		C	0.525	23.950	0.524	6.263
	2-2	D	0.534	23.600	0.543	6.511

Table 3. 1 CM^2 IL-MIS Solar Cells with 4% to 6% Efficiencies

Substrate Resistivity Ω-cm	Cell ID		Experimental Results			
			V_{oc} (V)	I_{sc} (mA)	FF	% EFF
1.2	9-1	A	0.566	29.200	0.317	5.008
	9-2	A	0.557	28.050	0.353	5.275
		C	0.555	27.450	0.324	4.730
0.7-1.3	1-1	B	0.491	24.400	0.475	5.412
		C	0.482	20.700	0.451	4.280
0.7-1.3	3-1	A	0.536	26.450	0.421	5.674
		B	0.525	25.000	0.417	5.212
	3-2	A	0.531	25.550	0.407	5.255
		C	0.537	25.400	0.354	4.592
0.7-1.3	T-2	D	0.542	28.300	0.330	4.811
8.0-12.0	2-3	A	0.496	27.050	0.404	5.150
		K	0.505	28.100	0.331	4.463
0.7-1.3	92-2	A	0.533	27.750	0.357	4.483
0.7-1.3	2	C	0.507	23.350	0.418	4.704
		D	0.505	24.100	0.409	4.734
0.7-1.3	4-1	C	0.524	23.050	0.379	4.350
	4-2	B	0.535	24.500	0.402	5.008

Table 4. 19 CM^2 IL-MIS Solar Cells

Substrate Resistivity Ω-cm	Cell ID	Thin Oxide Thickness (Average)	Experimental Results			
			V_{oc} (V)	I_{sc} (mA)	FF	% EFF
0.7-1.3	1-H	22Å	0.524	342.5	0.305	2.438
	1-WO	19Å	0.481	171.0	0.473	1.733
	1-M	19Å	0.452	128.6	0.466	1.208
	2-H	21Å	0.524	210.0	0.401	1.968
0.2-0.5	2-WO	19Å	0.482	153.6	0.447	1.476
	2-M	18Å	0.404	70.8	0.512	0.653
3.0-6.0	3-H	21Å	0.540	517.0	0.323	4.014
	3-WO	19Å	0.536	571.0	0.394	5.374
	3-M	18Å	0.531	534.0	0.384	4.855

3.0 A Comprehensive Analytical Model for Metal-Insulator-Semiconductor (MIS) devices

A detailed model for MIS devices has been developed that covers a wide range of parameters which include surface states, silicon dioxide thickness, substrate doping, fixed oxide charges, substrate thickness, and metal work function [3,4]. One of the main advantages of this model is the prediction of the range of the thin oxide thickness versus the maximum efficiencies of the MIS solar cells. In this model we have made the following three main assumptions:

1. The semiconductor charges Q_{sc} is calculated under non-equilibrium conditions, which can be written as:

$$Q_{sc} = \mp\sqrt{2KT\varepsilon_s N_A}\left[\beta\Psi_s + e^{-\beta\Psi_s} - 1 + \frac{n_i^2}{N_A^2}\left\{e^{\beta\phi_s}[e^{\beta\Psi_s} - 1] - \beta\Psi_s\right\}\right]^2 \quad (1)$$

The old expression to calculate Q_{sc} [9] assumes equilibrium condition for Q_{sc}. It gives expression like equation (1), but without the term $e^{\beta\phi_s}$.

$$Q_{sc} = \mp\sqrt{2KT\varepsilon_s N_A}\left[\beta\Psi_s + e^{-\beta\Psi_s} - 1 + \frac{n_i^2}{N_A^2}\left\{e^{\beta\Psi_s} - 1 - \beta\Psi_s\right\}\right]^2 \quad (2)$$

2. The tunneling factor ($\theta(\chi,\delta) = \exp\{\int |K| dx\}$) is calculated from the curves generated by Card [10,11] for $\int |K| dx = \chi^{1/2} d_i$ against d_i.

3. The permittivity of oxide is taken to be that of free space.

Without the first and second assumptions we could predict that maximum efficiencies occur at about $10\text{Å} < d_i < 15\text{Å}$ (the range of the thin oxide thickness is from 15Å to 25Å) and that the efficiency is very sensitive to the variation of the oxide thickness. If the efficiency is so sensitive as the old model claimed, higher efficiencies could not be obtained in practice. Our model includes the first and second assumption and predicts more practical results, which are shown in Table 5 and Figures 1 and 2. From Table 5 we see that for $d_i = 15\text{Å}$, the efficiencies with and without the first and second assumptions are nearly the same. That is why the old models can predict the efficiency correctly at this oxide thickness. When the thickness of the thin oxide is increased to 20Å our model gives 17.3% efficiency instead of 14.1% calculated without the first and second assumptions. If the thickness is increased to 25Å our model predicts 17.1% efficiency which is compared with 8.76% calculated without these assumptions. In our model the efficiency starts decreasing only with $d_i = 25\text{Å}$. This is clearly indicated in Figure 1. Figure 3 shows the 1-V characteristic of MIS solar cell for different oxide thickness with and without these assumptions. For the thin oxide in MIS contacts our model for MIS devices predicts more practical results [10,12,13,14]. This is particularly important when the thickness is increased to 25Å [4,14].

Table 5. Effects of the New Assumptions in our Model

Eq. #	d_i (Å)	-LN (θ)	ψ_s (V)	ϕ_s(V)	η (%)	FF(%)	V_{OC}(mV)	J_{SC}(mA/cm^2)
(1)	10	1.8	.6840	.0000	14.440	79.21	484.32	37.639
	15	4	.7552	.0000	17.165	81.70	558.13	37.644
	20	7.5	.7548	.0000	17.288	81.78	651.58	37.644
	25	13	.7497	.0057	17.120	80.96	561.75	37.644
(2)	10	10	.6831	.0039	16.587	81.00	544.77	37.639
	15	15	.7534	.0246	17.157	81.06	562.30	37.644
	20	20	.7431	.1516	14.117	66.69	562.35	37.643
	25	25	.7285	.2953	8.755	41.36	562.37	37.640

Calculation was made for $N_A = 2\times10^{15} cm^{-3}$, $\phi_m = 4.1\,V$, $H = 250\mu m$,

$$\varepsilon_i = 1,\ N_F = 5\times10^{11} cm^{-2}.$$

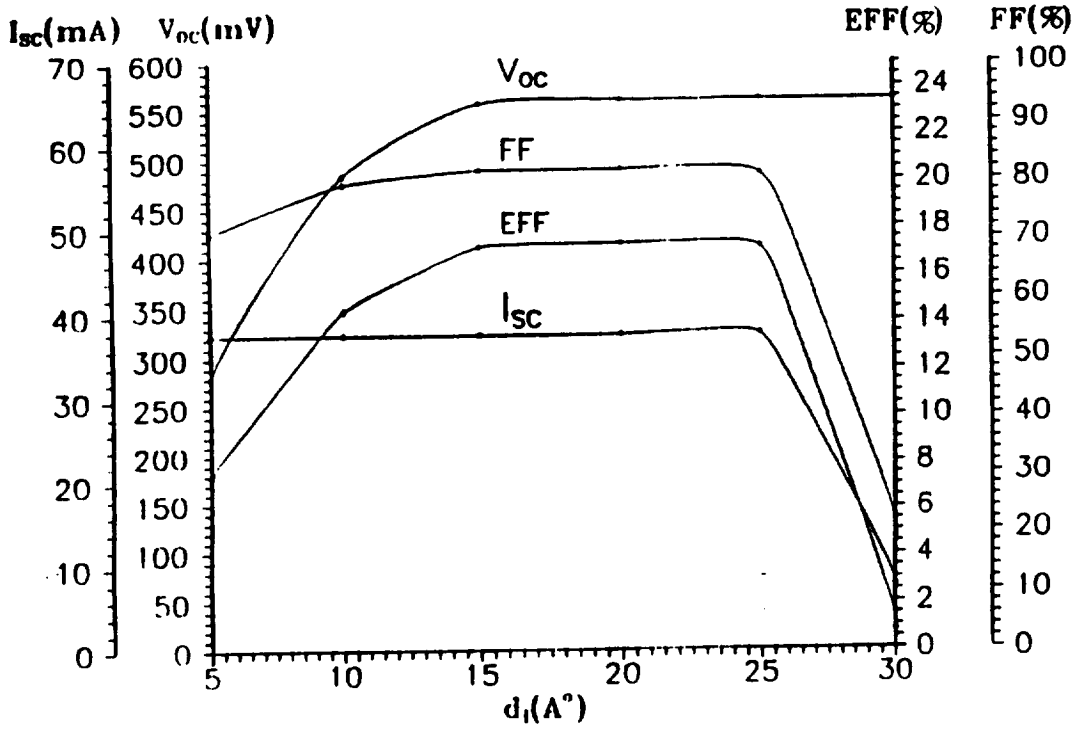

Figure 1: The efficiency, the open circuit voltage, the short circuit current, and the fill factor for the MIS solar cell for different oxide thicknesses d_i with the new assumptions.

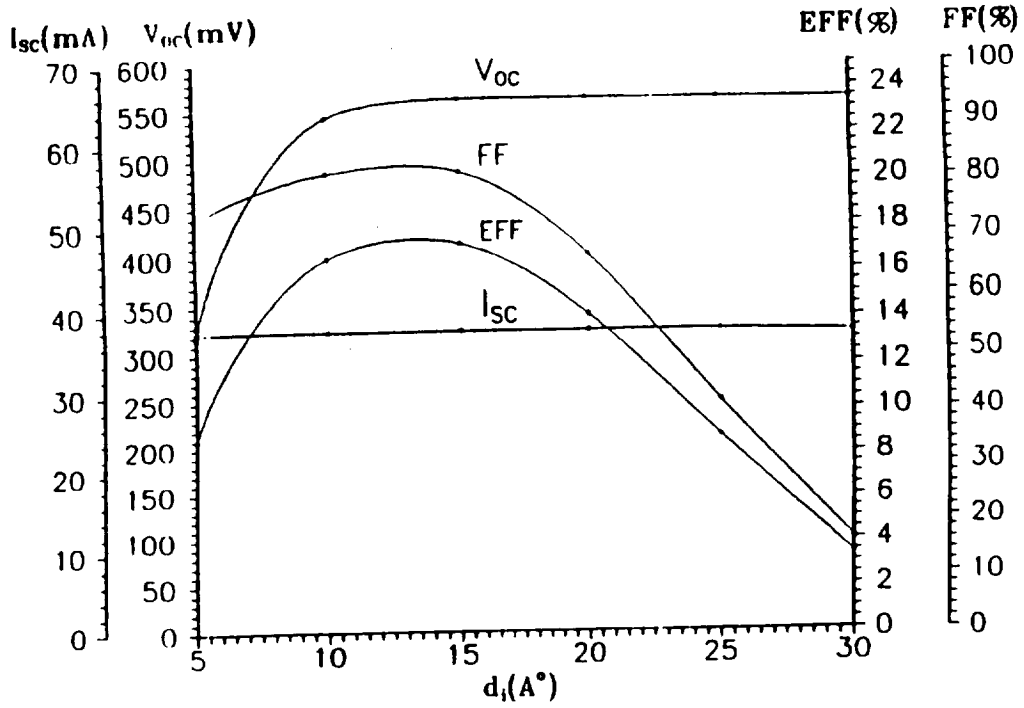

Figure 2: The efficiency, the open circuit voltage, the short circuit current, and the fill factor for the MIS solar cell for different oxide thicknesses d_i with equilibrium conditions and old tunneling factor.

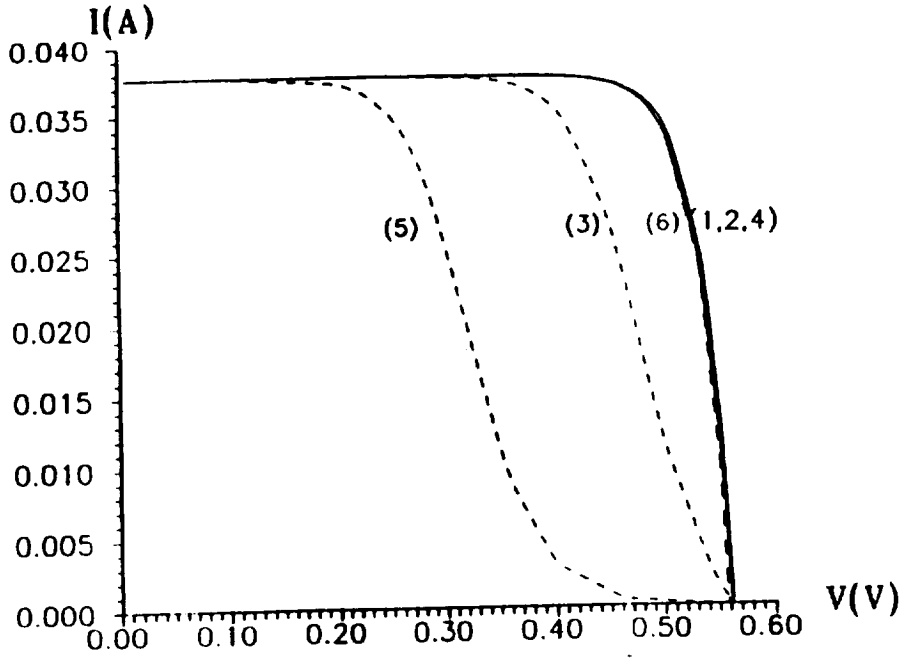

Figure 3: The I-V characteristics for MIS solar cells.
1) d_i = 15Å, equilibrium and old tunneling factor.
2) d_i = 15Å, non equilibrium and new tunneling factor.
3) d_i = 20Å, equilibrium and old tunneling factor.
4) d_i = 20Å, non equilibrium and new tunneling factor.
5) d_i = 25Å, equilibrium and old tunneling factor.
6) d_i = 25Å, non equilibrium and new tunneling factor.

The effect of the third assumption is illustrated in Table 6. As the permittivity of the thin oxide changes from 3.9 to 1 while fixing the metal work ϕ_m, the hole tunneling current J_{pt} increases; the electron tunneling current J_{nt} decreases; the diffusion current J_{dn}, the electron current through surface states J_{ns}, and the generation-recombination current in the depletion region J_{rg} increase. The increase of J_{dn}, J_{ns}, and J_{rg} causes a decrease in the fill factor. As the dark-current components increase, the efficiency, short-circuit current, and open-circuit voltage decrease.

The effect of this assumption is relatively small when the equilibrium conditions are satisfied. When the surface-state densities or the doping concentrations of the substrate are changed to get nonequilibrium conditions, the effect of permittivity values according to the third assumption is noticeable (see Table 6). The nonequilibrium conditions mean a substantial decrease in surface potential ψ, which leads to a bigger increase in the voltage drop across the insulator. The dark-current components become bigger and the device is forced deeper into nonequilibrium when the permittivity ε_i changes from 3.9 to 1. The efficiency, the fill factor, and the open-circuit voltage will be reduced. The same effect of changing ε_i can be noticed with changing thin oxide thickness d_i. For very thin thin oxide ($d_i < 10\,\text{Å}$) or very thick thin oxide ($d_i > 30\,\text{Å}$) the effect of the value of ε_i is significant because of the existence of the nonequilibrium conditions. But with $15\,\text{Å} < d_i < 25\,\text{Å}$ the near-equilibrium conditions occur and the effect of the value of ε_i is negligible on the performance of the MIS solar cells.

Table 6. Effects of Different Values of the Oxide Permittivity

ε_i	para-meter	ψ_s (V)	ϕ_s(V)	η (%)	FF(%)	V_{oc}(mV)	J_{sc}(mA/cm^2)
1	ϕ_m=4.1	.7548	.0000	17.288	81.777	561.58	37.644
	ϕ_m=4.7	.2798	.2914	4.222	60.624	185.21	37.602
3.9	ϕ_m=4.1	.7867	.0000	17.310	81.975	562.15	37.646
	ϕ_m=4.7	.2425	.3282	2.880	55.485	138.06	37.594
1	D_{it}=1.10^{10}	.7914	.0000	17.318	81.801	562.37	37.646
	D_{it}=5.10^{12}	.1932	.3536	.537	33.402	42.79	37.579
3.9	D_{it}=5.10^{10}	.8043	.0000	17.319	81.802	562.39	37.647
	D_{it}=5.10^{12}	.6232	.0033	13.949	79.146	468.30	37.635
1	N_A=2.10^{13}	.6392	.0000	13.231	78.223	442.56	38.221
	N_A=2.10^{17}	.5914	.0959	12.649	74.670	521.77	32.467
3.9	N_A=2.10^{13}	.6685	.0000	13.237	78.241	442.55	38.229
	N_A=2.10^{17}	.8269	.0001	17.022	82.375	636.29	32.476
1	N_F=10^9	.660	.0000	16.745	81.219	547.77	37.637
	N_F=10^{14}	1.057	.0008	17.351	81.694	562.36	37.768
3.9	N_F=10^9	.760	.0000	17.293	81.782	561.70	37.644
	N_F=10^{14}	1.056	.0000	17.388	82.293	562.41	37.569
1	H=50	.7548	.0000	13.372	80.563	520.86	31.867
	H=600	.7548	.0000	18.256	82.019	571.29	38.961
3.9	H=50	.7867	.0000	13.381	80.578	520.99	31.874
	H=600	.7867	.0000	18.287	82.042	572.80	38.962
1	d_i=10	.6840	.0000	14.440	79.211	484.32	37.639
	d_i=15	.7552	.0000	17.165	81.696	558.13	37.644
	d_i=20	.7548	.0000	17.288	81.777	561.58	37.644
	d_i=25	.7497	.0057	17.120	80.962	561.75	37.644
	d_i=30	.2704	.5566	.793	18.826	561.76	7.499
3.9	d_i=10	.7712	.0000	16.768	81.442	546.94	37.640
	d_i=15	.7900	.0000	17.274	81.774	561.13	37.644
	d_i=20	.7867	.0000	17.310	81.795	562.15	37.646
	d_i=25	.7827	.0017	17.255	81.529	562.18	37.646
	d_i=30	.4837	.3850	5.669	26.830	562.17	37.581

The effects of changing the values of parameters on the behavior of the MIS solar cells and MIS contacts are summarized as follows:

1. The Effects of Changing Metal Work Functions ϕ_m

The different values of work functions of metals, ϕ_m, affect the current-voltage characteristics of MIS contact under dark conditions. For ϕ_m less than a value of ϕ_{mc} ($\phi_m < \phi_{mc}$), the semiconductor is strongly inverted. The dominant component of current is the diffusion current for reverse bias and for small forward bias. For higher forward applied voltage, the MIS contact is driven to depletion, and the current becomes larger. The main component of current is now due to the recombination in the depletion region. The hole and electron tunneling currents through the thin oxide are negligibly small. For $\phi_m > \phi_{mc}$, the MIS contact is no longer at strong inversion, except for very high reverse bias. The dominant component of dark current is now that passes through the surface state J_{ps}. The diffusion current and the recombination current in depletion region become less important and can be neglected. The tunneling through surface states dominates and controls the behavior of the MIS contact. The dark current J_{dark} is approximately equal to the component that passes through the surface state J_{ps} [3]. The I-V characteristics of a MIS contact for different ϕ_m are illustrated in Figure 4.

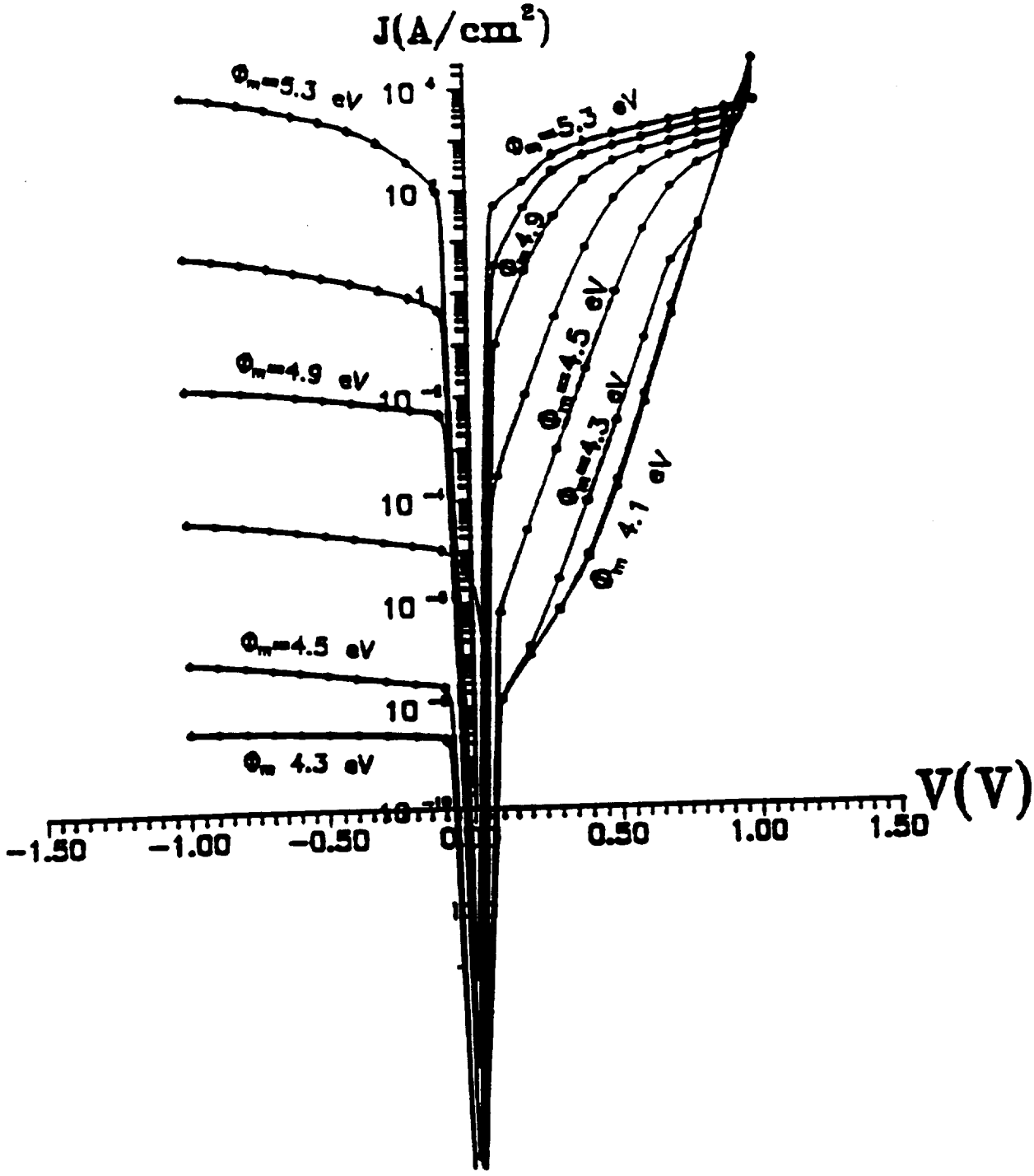

Figure 4: The I-V characteristics of a MIS contact for different metal work functions ϕ_m (eV).

For MIS solar cells the choice of the metal is essential. Figure 5 shows the effect of choosing metals with different work functions ϕ_m on the efficiency, the fill factor, the short-circuit current, and open-circuit voltage. For ϕ_m of less than a certain value (ϕ_{mc}) we get higher efficiency, increasing ϕ_m decreases the efficiency. Our calculations for dark conditions [3] show that $\phi_{mc} = 4.3\,\mathrm{V}$ under zero terminal voltage corresponds to the onset of strong inversion for the parameters used in our model. For lower $\phi_m < \phi_{mc}$, the split between the electron and hole Fermi levels ϕ_s is approximately equal to qV, where V is the terminal voltage. When the MIS cell is under illumination, the incident photons generate electron-hole pairs. The electrons go to the surface. Because the surface is initially strongly inverted, the concentration of electrons at the surface is not affected too much by the light and near equilibrium conditions can be assumed.

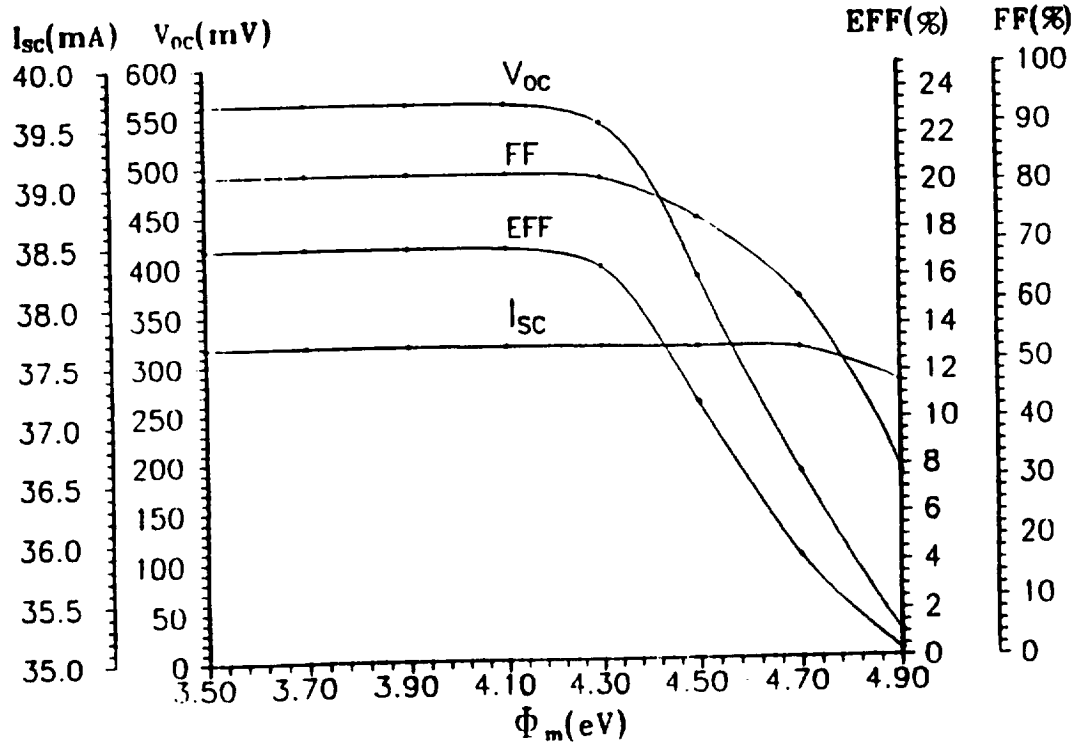

Figure 5: The efficiency, the open circuit voltage, the short circuit current, and the fill factor for the MIS solar cell for different metal work functions ϕ_m.

The current drawn from the cell can be written as $J_t = J_{light} - J_{dark}$ and $J_{dark} = J_{ps} + J_{pt} + J_{dn} + J_{rg}$ (J_{pt} is the hole tunneling current. J_{ps} is the electron current through surface state. J_{dn} is the diffusion current. J_{rg} is the generation recombination current in the depletion region.) For $\phi_m < \phi_{mc}$, ϕ_s is approximately equal to the terminal voltage and J_{ps} is small. The main component of the dark current is J_{dn} and the open-circuit conditions occur when $J_{dn} \cong J_{light}$. This leads to higher open-circuit voltage (V_{oc}), fill factor (FF) and efficiency (η). For $\phi_m > \phi_{mc}$ the tunneling current through surface states (J_{ps}) becomes the dominant current component. The open-circuit condition occurs when $J_{ps} \cong J_{light}$. It occurs at lower terminal voltage. The increase of ϕ_m increases J_{ps}. As a consequence, V_{oc} and efficiency η decrease and, hence, the fill factor decreases.

2. The Effect of Changing the Substrate Doping Concentration N_a

The doping concentrations of the silicon substrate affect the dark current of the MIS contact. There is a critical value N_{ac} under which the I-V characteristic follows the ideal diode equation. This N_{ac} is found to be around $10^{17} cm^{-3}$. For $N_a < N_{ac}$ the main components of dark current are the diffusion current J_{dn} for reverse and small forward bias, and the recombination current in depletion region J_{rg} for reverse bias. The I-V characteristics of a MIS contact for different N_a are illustrated in Figure 6. The main tunneling current is due to the minority carrier under the dark conditions.

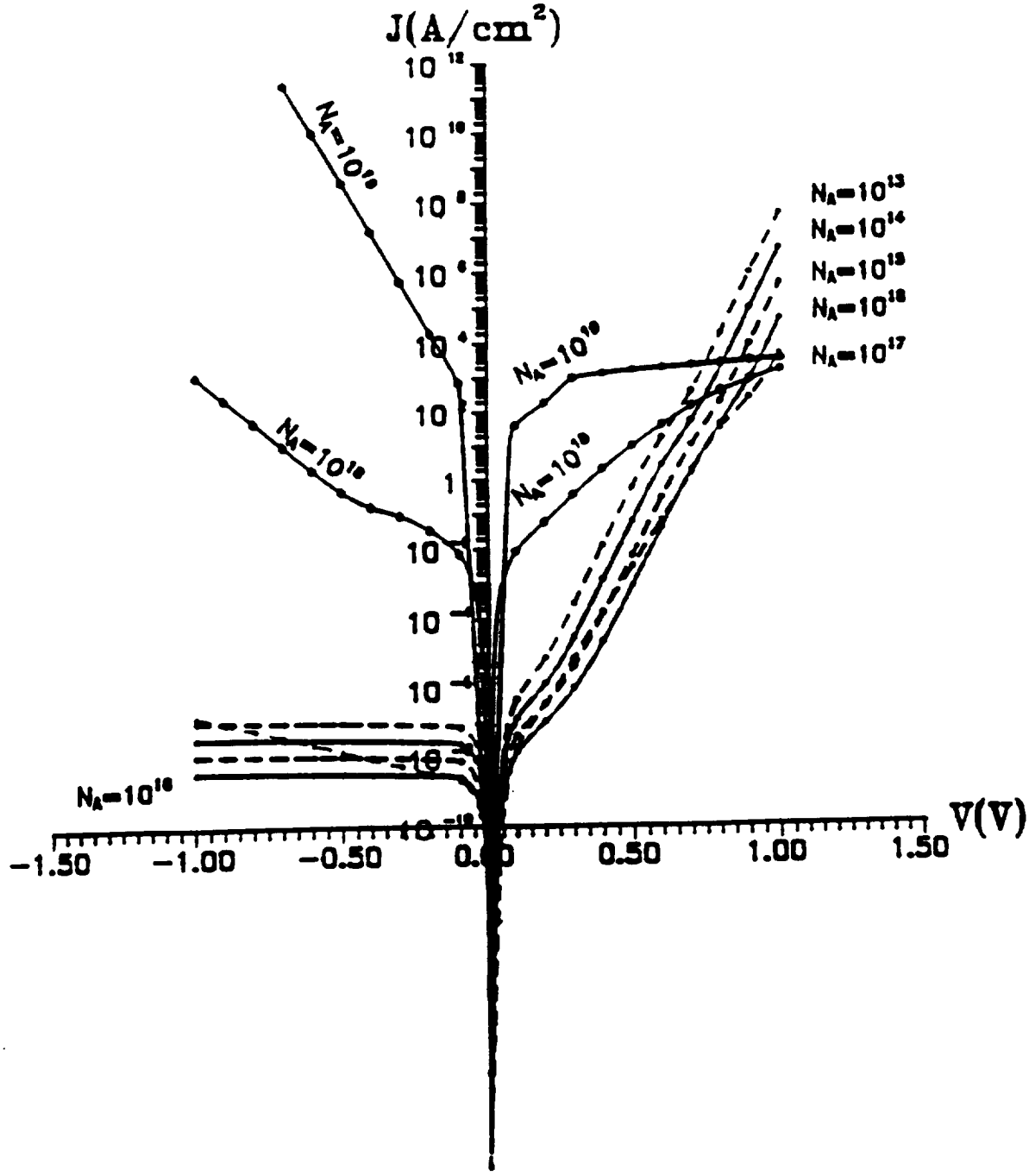

Figure 6: The I-V characteristics of a MIS contact for different doping densities N_A (cm^{-3}).

The dependence of efficiency, open-circuit voltage, short-circuit current, and fill factor on the substrate doping N_a is shown in Figure 7. The figure demonstrates that for a lightly doped substrate the efficiency is low. By increasing N_a the efficiency, the open-circuit voltage, and fill factor increase until they reach the peak for the range $N_a = 10^{15}$ to $10^{17} cm^{-3}$. Then, they start decreasing again. For the short-circuit current, it decreases while the doping is increased because the lifetime of minority carriers decreases with increasing N_a. Using a certain metal work function, the band bending Ψ_s increases with increasing N_a due to the increase of metal-semiconductor work function difference until a certain doping density ($N_a = 5 \times 10^{16} cm^{-3}$) is reached, which is called N_{ac}. For $N_a < N_{ac}$ the efficiency is increased due to the increase of band bending Ψ_s. In this case, the semiconductor surface is thermally inverted and equilibrium conditions occur. For $N_a > N_{ac}$ the semiconductor charges at the surface decrease until the effect of surface-state charges prevails, which leads to a decrease in Ψ_s until the inversion layer vanishes. For a similar reason like that for higher $\phi_m > \phi_{mc}$, the open-circuit voltage, efficiency, and fill factor become lower with increasing $N_a > N_{ac}$.

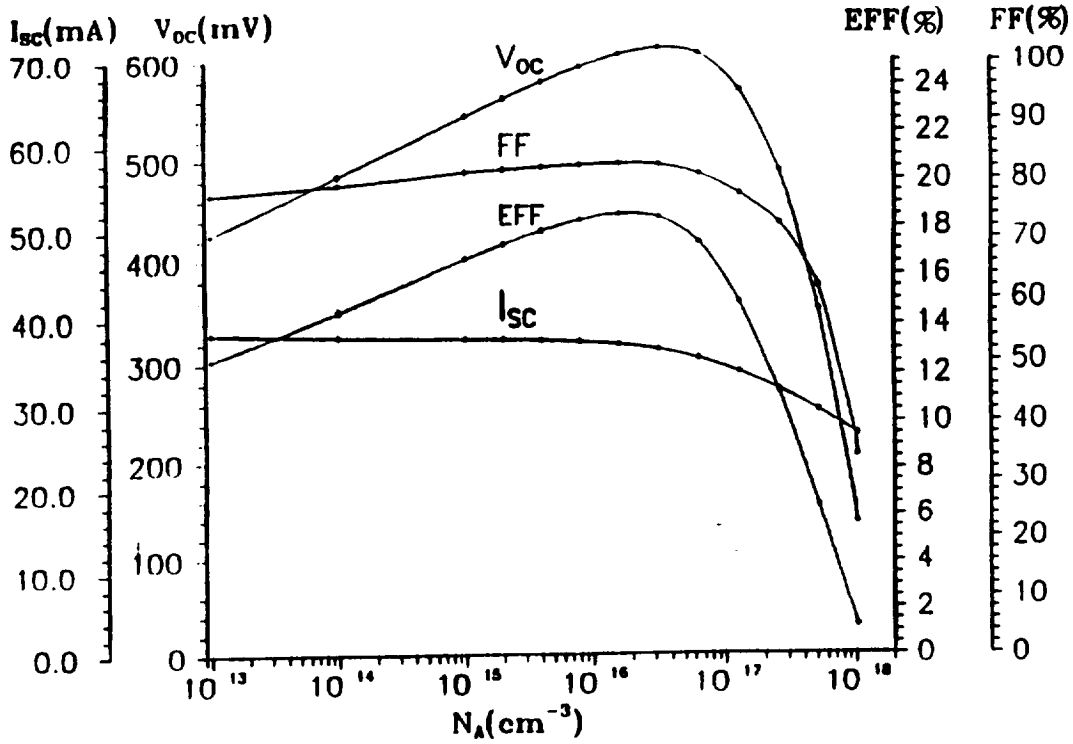

Figure 7: The efficiency, the open circuit voltage, the short circuit current, and the fill factor for the MIS solar cell for different doping densities N_A.

3. The Effect of Changing the Surface-State Density D_{it}

The effects of the surface-states density D_{it} depend mainly on the choice of other parameters (ϕ_m, N_a, d_i (the thickness of the thin oxide), etc.). For choosing nearly optimum parameters, we get an inverted semiconductor surface. Increasing the surface-states density decreases the band bending and causes a decrease of the surface potential Ψ_s. As a result the dark current component J_{pt} will increase and the minority-carrier tunneling current J_{nt} will decrease.

When D_{it} exceeds a certain level which is called D_{itc}, the effect of surface states as recombination centers disturbs the near-equilibrium conditions. The concentration of holes at the surface increases and the hole recombination current through the surface states (J_{ps}) and the hole tunneling current (J_{pt}) increase significantly. As a result, the dark current increases substantially with increasing D_{it}. Therefore, the efficiency, the fill factor, and the open-circuit voltage decrease as shown in Figure 8.

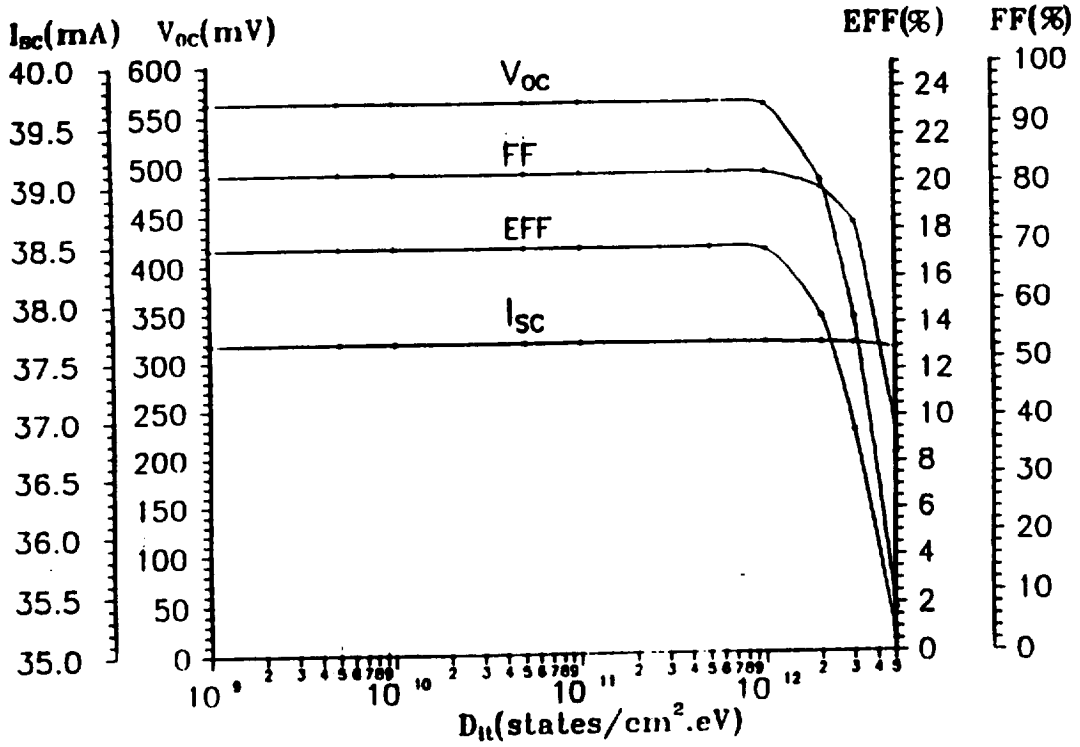

Figure 8: The efficiency, the open circuit voltage, the short circuit current, and the fill factor for the MIS solar cell for different surface states densities D_{it}.

As D_{it} increases further, the recombination current through surface states (J_{ps}) becomes very large even at short-circuit conditions. For good quality semiconductors using hydrogen annealing, the surface-state density is in the range of $10^{10} - 10^{11}\ states/cm^2 \cdot eV$, and their effect on the performance of the MIS solar cells is reduced if the other parameters (ϕ_m, N_a, N_f (the fixed oxide changes), d_i) are well chosen.

4. The Effect of Changing the Thin Oxide Thickness d_i

In our models we have studied the effects of changing the oxide thickness d_i which is an important parameter which affects the performance of MIS solar cells. Under dark conditions, the main components of current through the thin oxide in a MIS contact are J_{rg} (for reverse bias and small forward bias) and J_{Dn} (for large forward bias). The hole tunneling current J_{pt} is high, but less than J_{Dn}. As the thin oxide thickness d_i increases, the tunneling current J_{pt} drops substantially. This is shown in Figure 9.

In the case of MIS solar cells, the effects of changing d_i depends on the choice of the other parameters. Figure 1 shows the effect of d_i. For thinner oxide the hole tunneling becomes easier, which means that the dark current becomes larger. The total current becomes smaller and the open-circuit voltage is reduced and the efficiency decreases. As the thickness of the oxide layer increases, the hole tunneling through the insulator decreases which leads to a decrease in dark current. So the efficiency and open-circuit voltage increase until a certain thickness of oxide d_{ic} is reached. For $d_i > d_{ic}$, the electron tunneling becomes more difficult and higher concentration of photogenerated electrons exists in the semiconductor. As a result, an optically induced inversion layer is created and the split between electron and hole Fermi levels increases, so the dark current increases again. This causes a decrease in the open-circuit voltage and efficiency. When $d_i > d_{ic}$ and d_i reaches a certain value, the dark current becomes very large even at short-circuit conditions and the total current becomes very small (the short-circuit current J_{sc} decreases rapidly and reaches almost zero) as shown in Figure 1. For more detailed discussions see references [3] and [4].

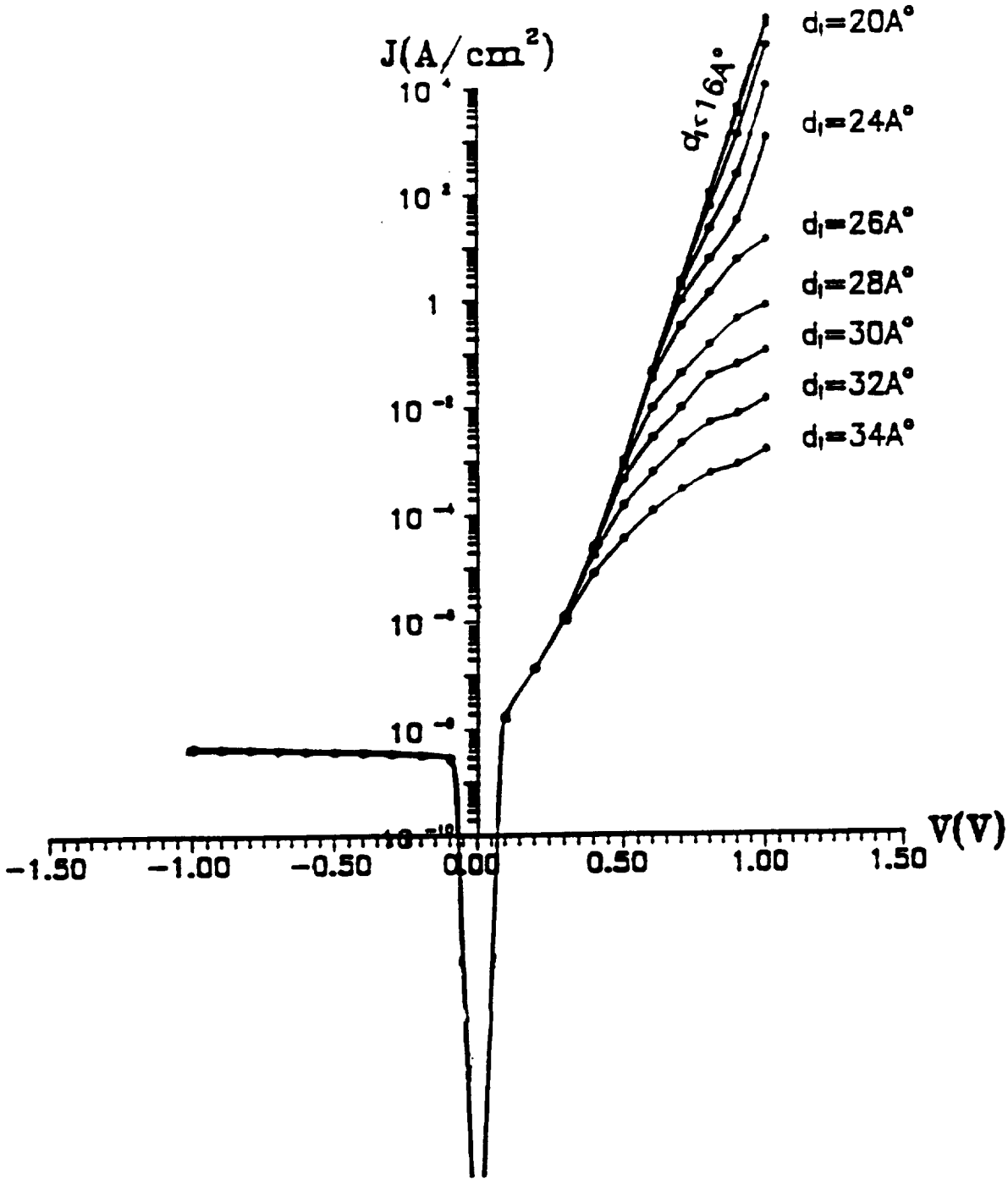

Figure 9: The I-V characteristics of a MIS contact for different oxide thicknesses d_i , for constant surface states D_{it} , and for metal work function $\phi_m = 4.1$ eV.

The most important parameters of the inverse layer MIS solar cells, for design consideration, include the doping concentration of the substrate and the thickness of the interfacial layer of the thin oxide in a MIS contact. Therefore, a lot of conclusions drawn from the study of MIS devices can be applied in the study of the inversion-layer MIS solar cells because MIS contacts are used in both cases.

4.0 The Two-Dimensional Model for the Inversion-Layer Metal-Insulator-Semiconductor (MIS) Solar Cells

A general purpose, two-dimensional, microelectronics device simulator using the finite element method has been developed [15]. This model is applied to the inversion-layer MIS solar cells. To model the MIS contacts the band to band tunneling currents and the current components due to the surface states need to be determined for the calculation of the dark current. The band to band currents have two components, one is the hole tunneling current and the other is the electron tunneling current. The hole tunneling current is

$$J_{pt} = A_p^* T^2 \theta(\chi_p, \delta)[e^{-\frac{E_{fp}-E_{vo}}{KT}} - e^{-\frac{E_{fm}-E_{vo}}{KT}}] \tag{3}$$

The electron tunneling current is

$$J_{nt} = A_n^* T^2 \theta(\chi_n, \delta)[e^{-\frac{E_{co}-E_{fm}}{KT}} - e^{-\frac{E_{co}-E_{fn}}{KT}}] \tag{4}$$

where $\theta(\chi, d_i) = \exp(-\chi^{1/2} d_i)$, which is the tunneling factor $\theta(\chi, d_i) = \exp\{\int |K| dx\}$ [16] for $\int |K| dx = \chi^{1/2} d_i$, and the curves from Card [10,11] are used to obtain $\chi^{1/2} d_i$. A_p^* and A_n^* are effective Richardson constants for holes and electrons, respectively. $\chi_n(\chi_p)$ is an effective potential barrier of oxide to electron (hole) tunneling into metal.

The surface-states current components include the electron current through surface states and the hole current through surface states. The former can be expressed as

$$J_{ns} = qD_{it}V_{th}\sigma_n[(1-f_t)n_s - f_t n_1] \tag{5}$$

The latter can be written as

$$J_{ps} = qD_{it}V_{th}\sigma_p[f_t p_s - (1-f_t)p_1] \tag{6}$$

In equations (5) and (6)

$$n_1 = N_c e^{\frac{E_{ss}-E_{co}}{KT}} \tag{7}$$

$$p_1 = N_v e^{-\frac{E_{fn}-E_{vo}}{KT}} \tag{8}$$

$$n_s = N_c e^{\frac{E_{fn}-E_{co}}{KT}} \tag{9}$$

$$p_s = N_v e^{-\frac{E_{fp}-E_{vo}}{KT}} \tag{10}$$

$$f_t = \frac{\tau_t f_{t0} + \tau_s f_m}{\tau_t + \tau_s} \tag{11}$$

$$f_{t0} = \frac{n_s\sigma_n + p_1\sigma_p}{(n_s+n_1)\sigma_n + (p_s+p_1)\sigma_p} \tag{12}$$

$$\tau_t = \tau_o e^{\chi^{1/2}d_t} \tag{13}$$

$$\tau_s = \frac{1}{V_{th}[(n_s+n_1)\sigma_n + (p_s+p_1)\sigma_p]} \tag{14}$$

$$f_m = \frac{1}{1+e^{\frac{E_{ss}-E_{fm}}{KT}}} \tag{15}$$

At the silicon oxide interface, the diffusion current becomes [17]

$$J_{Dn} = \frac{qD_n}{L_n} n_{po} \frac{F_2(H)}{F_1(H)} [e^{\beta\phi_s} - 1] \tag{16}$$

where

$$F_1(H') = \frac{S_n L_n}{D_n} \sinh\frac{H'}{L_n} + \cosh\frac{H'}{L_n} \tag{17}$$

$$F_2(H') = \frac{S_n L_n}{D_n} \cosh\frac{H'}{L_n} + \sinh\frac{H'}{L_n} \tag{18}$$

The generation recombination current in the depletion region can be written as

$$J_{rg} = \frac{qn_i \sqrt{\frac{2\varepsilon_s \psi_s}{qN_A}}}{\tau_n} [e^{(\beta\phi_s)/2} - 1] \tag{19}$$

All these current components are shown in Figure 10. In this diagram the Fermi levels for electrons and holes are split with energy difference equal to $q\phi_s$, the voltage drop across the insulator is Δ, the band bending is ψ_s, the neutral level for surface states is E_{ss}.

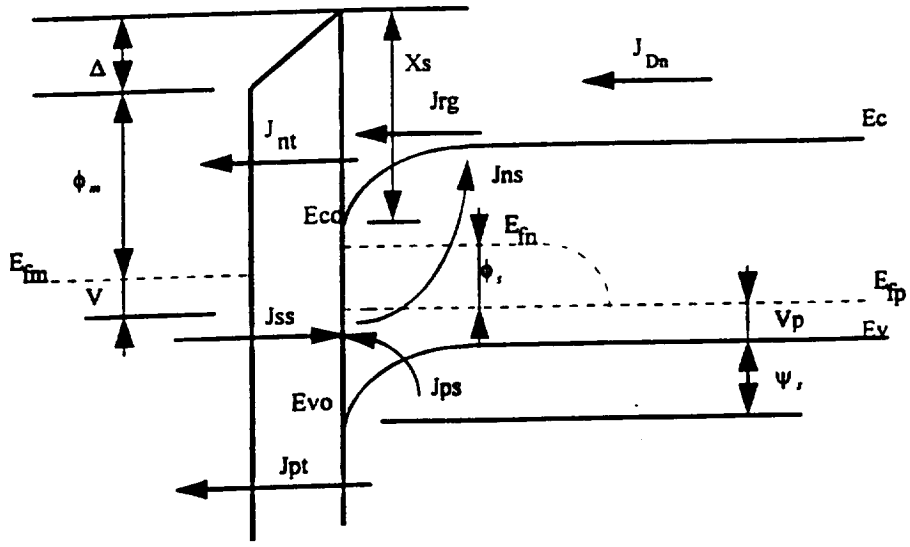

Figure 10: Energy band diagram for MIS contact.

The voltage drop across the oxide can be written as

$$\Delta = E_g + \chi_s - \phi_m - V_p - \psi_s - V \tag{20}$$

where V is the terminal forward bias.

The dark current in this simulation is obtained by

$$J_{dark} = J_{nt} + J_{pt} - J_{ns} + J_{ps} \tag{21}$$

where J_{nt} is the electron tunneling current, J_{pt} is the hole tunneling current, J_{ns} is the electron current through surface states, and J_{ps} is the hole current through surface states.

The effect of light is treated as a generation term which is given by

$$g(x) = \int_o^\infty [1 - R(\lambda)]\alpha(\lambda) N_m(\lambda) \exp(-\alpha(\lambda)x) d\lambda \tag{22}$$

where $N_m(\lambda)$ is the mass (m) photon flux spectrum, $\alpha(\lambda)$ is the silicon absorptivity, and $R(\lambda)$ is the optical reflection of the cell's front surface at the wavelength (λ) [18].

Figure 11 is a partial mesh of the inversion layer MIS solar cell. The equations for

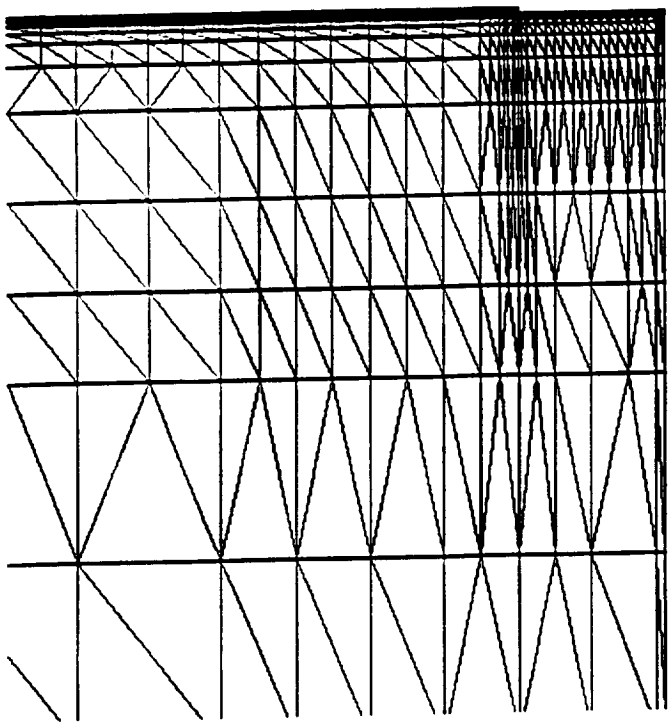

Figure 11: Partial mesh of the inversion-layer MIS solar cell.

tunneling currents and for surface state currents (Eqs. (3) to (6)) are applied to the thin oxide area which is between the metal and the silicon in the cells. The diffusive and drift current densities are calculated by Two-Dimensional General Purpose Finite Element Microelectronic Device Simulator [15].

The simulation of the inversion layer MIS solar cell using this two-dimensional microelectronic device simulator is a very difficult task. The very thin oxide layer between metal and semiconductor is about $20\,\mathring{A}$, which is much smaller than the cell dimension used in this simulation ($300\ \mu m \times 80\ \mu m$). This is very difficult for the numerical calculation.

The values of the parameters used in this simulation are shown in Table 7. The simulation results of the short circuit currents for different thickness of the thin oxide are shown in Table 8. The simulation results do not agree with the experimental values [19]. The problems come from the simulation of tunneling currents. More time is needed to have a further study on the effects of the inversion layer, the surface states, and the tunneling in the MIS contacts.

Table 7. Short Circuit Currents for Different Thickness of Tunneling Area [15]

(χ is the barrier potential for tunneling area, δ is the thickness of tunneling area)

tunneling area thickness	$\chi^{1/2}\delta$ ($eV^{1/2}$Å)	short circuit current (A/cm^2)
15 Å	2.7	no convergence
20 Å	7.5	0.337
30 Å	12.5	0.124

Table 8. Parameters Used in Simulation

PARAMETER	VALUE	UNIT
D_{it}	6.0 E11	states/cm^2/eV
V_{th}	0.0256	V
N_A	2.0 E15	/cm^3
N_f	5.0 E11	cm^{-2}
ϕ_m	4.1	V
d_i	20	Å
A_n^*	112	A/cm^2.K^2
A_p	32	A/cm^2.K^2
E_{ss}	0.33	eV
n_i	1.45 E10	/cm^3
σ_n	1.0 E-15	cm^2
σ_p	1.0 E-15	cm^2

5.0 Results and Discussion

Many 1 cm^2 inversion layer MIS solar cells have been fabricated. Most of them have low efficiencies, small short circuit currents, and small values of filled factors. There are eighteen 1 cm^2 IL/MIS cells which have the efficiencies between 6% and 7%, and there are four 1 cm^2 cells which have the efficiencies between 8.06% and 8.9%. The highest short circuit current is 30.400 mA while the largest open-circuit voltage obtained is 0.575V.

The performance of the $19cm^2$ cells is poorer than that of the 1 cm^2 cells. The best $19cm^2$ IL/MIS cell has $V_{oc} = 0.536\,V$, $I_{sc} = 571mA$, $FF = 0.394$, and 5.374% efficiency.

The growth of the thin oxide in the IL/MIS solar cells has been successful. The thin oxide in the range from 18Å to 25Å was successfully grown. Our analytical model for Metal-

Insulator-Semiconductor (MIS) devices is very successful to predict the effect of the thickness of the thin oxide on the efficiencies of the MIS solar cells, which is applicable to the IL/MIS solar cells.

A lot of efforts have been made to develop a two-dimensional model for the IL/MIS solar cells. Unfortunately it has not been successful. More work is necessary to develop the two-dimensional simulator for these photovoltaic devices.

References

1. Fat Duen Ho, "Further Study of Inversion-Layer MIS Solar Cells," Final Report submitted to MSFC, 1992.

2. Patrick D. McManus and Fat Duen Ho, "NASA Technical Memorandum," June 1994.

3. M. Y. Doghish and Fat Duen Ho, "A Comprehensive Analytical Model for Metal-Insulator-Semiconductor (MIS) Devices," *IEEE Trans. on Electron Devices*, Vol. 39, No. 11, pp. 2771-2780, 1992.

4. M. Y. Doghish and Fat Duen Ho, "A Comprehensive Analytical Model for Metal-Insulator-Semiconductor (MIS) Devices: A Solar Cell Application," *IEEE Trans. on Electron Devices*, Vol. 40, No. 8, pp. 1446-1454, 1993.

5. P. van Halen, R. E. Thomas, R. Mertens, and R. van Overstraeten, "Inversion-Layer Silicon Solar Cells with MIS Contact Grids," *Proc. 12th IEEE Photovoltaic Specialists Conference*, pp. 907-912, Nov. 1976.

6. G. C. Salter and R. E. Thomas, "Silicon Solar Cells Using Natural Inversion Layer Found in Thermally-Oxidized P-Silicon," *Solid State Electronics*, Vol. 20, pp. 95-104, 1977.

7. C. E. Norman and R. E. Thomas, "Inversion Layer Solar Cells with 10-12% AMI Efficiencies," *Proc. 12th IEEE Photovoltaic Specialists Conference*, pp. 993-996, Nov. 1976.

8. P. van Halen, R. Mertens, R. van Overstraeten, R. E. Thomas, and J. van Merbergen, "New TiOx-MIS and SiO_2-MIS Silicon Solar Cells," *IEEE Trans. on Electron Devices*, Vol. ED-25, No. 5, pp. 507-511, 1978.

9. P. Chattopadhyay and A. N. Daw, "Effect of Surface States on the Barrier Height in MIS Diodes in the Presence of Inversion," *International Journal of Electronics*, Vol. 58, No. 5, pp. 775-779, 1985.

10. H. C. Card, "Photo-Voltage Properties of MIS-Schottky Barriers," *Solid State Electronics*, Vol. 20, pp. 971-976, 1977.

11. K. K. Ng and H. C. Card, "Asymmetry in the SiO_2 Tunneling Barriers to Electrons and Holes," *J. Appl. Phys.*, Vol. 51, No. 4, p. 2135, 1980.

12. P. Viktorovitch and G. Kamarinos, "Improvement of the Photovoltaic Efficiency of Metal-Insulator-Semiconductor Structure: Influence of Interface States," *J. Appl. Phys.*, Vol. 48, No. 7, July 1980.

13. G. P. Srivastava, R. K. Bhatnagar, and S. R. Dhariwal, "Theory of Metal-Oxide-Semiconductor," *Solid State Electronics*, Vol. 22, pp. 581-587, 1979.

14. F. D. Ho and P. D. McManus, NASA/MSFC Laboratory Report, SCHO #13, 1989.

15. C. L. Sung, "A Two-Dimensional General Purpose Finite Element Microelectronic Device Simulator," Dissertation, The University of Alabama in Huntsville, 1996.

16. A. G. O'Neal, "An Explanation of the Asymmetry in Electron and Hole Tunnel Currents Through Ultra-Thin SiO_2 Films," *Solid State Electronics*, Vol. 29, pp. 305-310, 1986.

17. H. J. Hovel, "Semiconductors and Semimetals," Vol. 11: Solar Cells. New York: Academic Press, 1975.

18. C. E. Norman and R. E. Thomas, "Detailed Modeling of Inversion-Layer Solar cells," *IEEE Trans. on Electron Devices*, Vol. ED-27, No. 4, pp. 731-737, April 1980.

19. P. DeVisschere, "Two-Dimensional Modeling of the MIS Grating Solar Cell," *IEEE Trans. on Electron Devices*, Vol. ED-30, No. 7, pp. 840-849, July 1983.